INSTITUTE OF PHYSICS PUBLISHING JOURNAL OF PHYSICS G: NUCLEAR AND PARTICLE PHYSICS

J. Phys. G: Nucl. Part. Phys. **30** (2004) R57–R82 PII: S0954-3899(04)57170-0

TOPICAL REVIEW

Microsecond isomers in the magic regions ^{78}Ni and ^{132}Sn

J A Pinston and J Genevey

Laboratoire de Physique Subatomique et de Cosmologie, IN2P3-CNRS/Université Joseph Fourier, F-38026 Grenoble Cedex, France

E-mail: pinston@lpsc.in2p3.fr

Received 21 October 2003
Published 8 January 2004
Online at stacks.iop.org/JPhysG/30/R57 (DOI: 10.1088/0954-3899/30/2/R02)

Abstract

This paper reviews the status of the microsecond isomer spectroscopy in the vicinity of the doubly magic nuclei ^{78}Ni and ^{132}Sn. The various experimental techniques used for producing these isomers and for studing their γ and conversion-electron decay are discussed. The recently measured data on the energy levels and the electromagnetic transition rates have considerably increased the nuclear structure information in these two magic regions. They provide the opportunity for testing the predictive power of the shell model far away from the line of stability.

1. Introduction

The doubly closed shell nuclei ^{78}Ni and ^{132}Sn are very far from the line of stability. Moreover, above ^{48}Ca, they are the only magic nuclei now experimentally accessible in the neutron-rich region of the nuclear chart. The study of these nuclei and their neighbours is of special interest, as is shown by the attention given to them in recent papers. These new experimental data offer an opportunity for testing the basic ingredients of the shell-model calculations, such as the effective interactions between nucleons, far away from the valley of stability and to detect any departures from the shell model.

Located far from the stability line, these nuclei are very difficult to produce. Among the methods used for their production, thermal-neutron-induced fission and the spontaneous fission sources of ^{252}Cf and ^{248}Cm played initially the most important role. More recently, deep inelastic, fragmentation and fission at intermediate and relativistic energies have also been used.

A very broad spectrum of complementary experimental techniques is used to study the nuclear structure of these neutron-rich nuclei. Among them the search for microsecond isomers and the study of their decay schemes are very powerful tools, and in many cases it is the only way to get nuclear structure information for nuclei very far from the stability line. In the

vicinity of doubly magic nuclei these isomers are very abundant and they are generally yrast traps carrying considerable amounts of angular momentum. Moreover, they may be measured with recoil-fragment spectrometers which are efficient for the selection of the reaction products of interest. In this case, the detection is based on event-by-event time correlation between the fragments and the delayed γ-rays or conversion electrons de-exciting the isomers. This method allows one to detect the microsecond isomers produced at a very low rate and it is the most frequently used technique in recent experiments. Moreover, the measured energies and half-lives of the isomeric transitions allow one to deduce the electromagnetic transition rates, which are important to test theoretical models.

Microsecond isomer spectroscopy is complementary to prompt γ measurements with large detector arrays such as EUROBALL or GAMMASPHERE or β-decay experiments. As usual, it is only the combination of various experimental techniques and theoretical approaches which can give the full picture of the underlying nuclear structure. However, in this paper we have tried to emphasize the special role played by the microsecond isomers in this quest and have deliberately reduced the role of the other methods.

The paper is organized as follows: section 2 describes the experimental methods used to produce the microsecond isomers and to study their decay, while in section 3 the results of the measurements are reported; in section 4, the experimental level schemes are compared with the various shell-model calculations using empirical or realistic effective interactions; the electromagnetic transition probabilities are discussed in sections 4 and 5; section 6 contains a summary and the conclusions.

2. Experimental procedures

In this section some aspects of the experimental methods used to study microsecond isomer spectroscopy in very neutron-rich nuclei of the ^{78}Ni and ^{132}Sn regions are discussed. These isomers are produced by different reactions. Deep-inelastic binary collisions are used for the study of stable and moderately neutron-rich nuclei. Angular momenta up to 20 $\hbar$ can be transferred in these reactions. For the most neutron-rich nuclei the fission process is used. However, more recently fission and fragmentation of high-energy heavy ions were also exploited. Angular momenta up to 15 $\hbar$ can be transferred in these reactions.

Thick- and thin-target methods are used. In the latter case, recoil-fragment spectrometers are used to select the products of interest in-flight. The detection is based on the event-by-event time correlations between the fragments and the delayed γ-rays or conversion electrons de-exciting the isomers. This method allows one to detect microsecond isomers produced at a very low rate and it has been frequently used in recent works.

With these experimental techniques, the following information can usually be obtained: γ-ray and conversion-electron energies and intensities, γ–γ or γ–e coincidences, half-lives of the isomeric transitions and isomeric yields. In many cases the reduced transition probabilities for isomeric transitions can be directly deduced from the above quantities.

2.1. Thick target experiments

2.1.1. Reactor plus isotope separator. In the past, several isotope separators were built to isolate nuclei with known masses and to measure the radiation associated with their decays. The very neutron-rich nuclei are produced through fission reactions, with neutrons of reactors impinging on various thick targets of ^{233,235,238}U. The reaction products which are stopped in the target diffuse out of the surface, reach an ionizer and are extracted. The beam is

mass-analysed and the decay of the products is measured at the exit of the spectrometer. The short-lived isomers are detected by γ–γ–t or β–γ–t delayed-coincidence techniques.

In the Sn region, the microsecond isomers in the even ^{128,130}Sn were observed for the first time by Fogelberg *et al* [1] at the OSIRIS facility in Studsvik. Microsecond isomers were also measured in the odd-mass $A = 127$ and 129 [2] at the same facility, although their isotopic identification was not firmly established. Other microsecond isomers were observed in ^{127}Sb [3] and ^{128}In [4].

More recently, at the OSIRIS facility, high-spin millisecond isomers were also found in ^{131}Te (93 ms), ^{125}In (5.0 ms) and ^{129}In (110 and 700 ms) [5].

2.1.2. Measurements with large γ-ray detector arrays. Large arrays of γ-ray detectors such as GAMMASPHERE, EUROGAM2 or EUROBALL3 were used to measure the prompt and delayed γ-rays of fission fragments (FFs). These FFs are produced by spontaneous fission of ^{252}Cf or ^{248}Cm or by fission induced by heavy ions on heavy targets. The technique generally used involves observing the multi-fold γ-ray coincidences between several detectors. The time window in these experiments is in the range 5–500 ns or 5–1000 ns. For instance, the decay of the 80 ns half-life isomer in the very neutron-rich ^{134}Sn [6] was measured with this technique.

New experiments [7, 8] were recently performed to detect FFs in coincidence with delayed γ-rays. For this purpose the two FFs were detected by photovoltaic cells of the SAPHIR detector while the γ-rays were detected with EUROGAM2 or EUROBALL3. The mass numbers of the FFs are extracted from their energies. The γ-rays are measured in a time window of 1 μs after fission.

All these experiments measure isomers with half-lives shorter than 1 μs and are complementary to the other measurements performed with recoil spectrometers which generally measure longer half-lives due to the long flight paths of the FFs.

2.1.3. Deep-inelastic reactions at Argonne. This technique has been used at Argonne to study microsecond isomers in the semi-magic Sn nuclei in the mass range $A = 119$ to 126 [9–12]. These isotopes were produced at the ATLAS superconducting linear accelerator by deep-inelastic reactions, using pulsed beams of ^{76}Ge, ^{80}Se, ^{136}Xe and ^{238}U on lead-backed ^{122,124}Sn targets with energies 10–15% above the Coulomb barrier. A 1 mg cm^{-2} target was placed at the centre of the Argonne–Notre Dame γ-ray facility, which consisted of 12 Compton-suppressed detectors and an inner ball of BGO hexagons. The Ge detectors recorded off-beam γ-ray singles spectra in a two parameter E_γ versus time mode, as well as off-beam γ–γ prompt coincidence events. The time interval between a Ge detector pulse and the firing (up to 10 μs later) of a BGO hexagon was also recorded.

In these experiments there is no A and Z identification of the reaction fragments and making an isotopic assignment for the unknown γ-ray cascades proves to be a difficult problem. This assignment is based (i) on rare overlap with β-decay data or (ii) on the relative yields obtained with different beams.

Similar techniques were used to study microsecond isomers in ^{128}Te and ^{130}Te [13], produced from the reaction ^{130}Te + 275 MeV ^{64}Ni, and using the GASP Ge detector array at Legnaro (Italy).

2.2. Thin target experiments

The pioneering works using this technique were performed with the recoil fragments spectrometer JOSEF. The fragments were produced by thermal-neutron-induced fission on

^{235}U targets in the reactor FRJ-2 in Jülich, Germany, in a neutron flux of 10^{14} n cm^{-2} s^{-1}. Both γ- and x-rays of the isomers were measured by Ge- and Si(Li)-detectors, respectively. In the first experiment performed in 1970 [14], 15 new microsecond isomers were reported, mainly in the $A = 100$ region and in the vicinity of ^{132}Sn. These isomers have half-lives ranging between 0.1 μs and 100 μs.

At present, the search for microsecond isomers may be performed with three recoil fragment spectrometers, FRS at GSI, LISE3 at GANIL and LOHENGRIN at ILL. The energies of the recoiling fragments are very different at these three facilities, 700–1000 MeV/nucleon at FRS, about 60 MeV/nucleon at LISE3 and 70 MeV total energy at LOHENGRIN. This leads to different advantages and disadvantages for microsecond isomer spectroscopy. A high velocity allows complete event-by-event A and Z identification of the fragments, while only A identification is achieved for heavy fragments close to ^{132}Sn having a low velocity. In contrast, a low velocity is suitable to stop the fragments without producing secondary reactions and high multiplicity x-ray or δ-electron background. Moreover, in this case the fragments can be stopped in a very thin layer of material which is suitable to detect very low-energy γ-rays or conversion electrons.

2.2.1. LISE3 at GANIL. A detailed description of the experimental method used for identification and study of short-lived isomers can be found in the paper of Grzywacz *et al* [15]. The microsecond isomers near ^{78}Ni are produced by fragmentation of an ^{86}Kr beam of 60 MeV/nucleon, on a $\mathrm{Ni_{natural}}$ target. The separation of the fragments is achieved by means of the Alpha-LISE3 spectrometer. The ion detector is a telescope made of several planar silicon detectors. The event-by-event measurements of the $B\rho$ of the spectrometer, energy loss (ΔE) and total kinetic energy in the silicon detectors, and time of flight between a ΔE detector and the cyclotron radio frequency allow for an unambiguous A, Z and Q identification of the transmitted nuclei. The delayed γ-rays emitted by the fragments implanted in the last detector of the telescope are detected by several large volume Ge detectors in close geometry. Two flight paths of 17 and 131 m are used, the corresponding time of flight being 0.2 and 1.2 μs, respectively.

A comparison [16] of an ungated identification spectrum, Z versus A/Q, with a spectrum gated by the delayed γ-rays is displayed in figure 1. It shows the presence of a large number of microsecond isomers.

2.2.2. FRS at GSI. Neutron-rich microsecond isomers near ^{132}Sn are produced by projectile fission of ^{238}U at the relativistic energy of 750 MeV/nucleon impinging on a 1 g cm^{-2} Be target. The ions of interest are separated by combining magnetic analysis and energy loss in a degrader. This wedge-shape degrader, with a thickness set to 50% of the range of the selected fragments, is placed in the middle plane of the spectrometer. For each production setting of the spectrometer, some 12 to 20 different fragment species were transmitted to the final focal plane. They are slowed down using an adjustable Al degrader of about 6 g cm^{-2} and subsequently implanted in a 6.5 mm thick Al foil. The catcher is surrounded by four segmented clover detectors used for the detection of the delayed γ-rays de-exciting the isomers.

The separated ions are identified event-by-event via combined time-of-flight, position-tracking and the energy-loss measurement. The flight time of the ions through the separator is about 0.3 to 0.4 μs.

From these initial experiments, it seems that the beam intensity of the FFs produced at GSI in the ^{132}Sn region is very low and only the decay scheme of one new microsecond isomer,

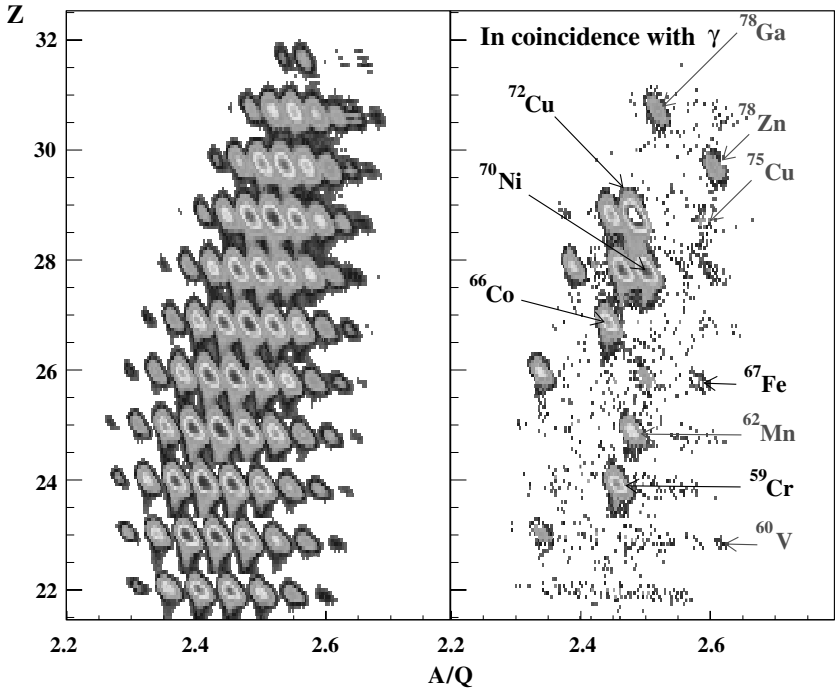

Figure 1. Typical heavy-ion identification plots: raw (left) and gated by delayed γ-rays (right) obtained in the reaction 60.6 MeV/nucleon ^{86}Kr on a Ni target (from [16]).

^{136m}Sb [17], has been reported in the literature up to now. However, this facility is much more powerful in other mass regions, especially in the vicinity of ^{208}Pb where it has no competitor.

2.2.3. LOHENGRIN at ILL. The nuclei are produced by thermal-neutron-induced fission of ^{239}Pu and ^{241}Pu. These targets are chosen to optimize the production rate for a particular nucleus of interest. The ^{241}Pu target is the most efficient for producing the most neutron-rich nuclei, especially in the ^{132}Sn region and has a high fission cross section of about 1000 b. In many cases the fission yields from thermal neutrons on ^{241}Pu are higher than in the reaction involving fast neutrons on ^{238}U.

A detailed description of the experimental method used for the identification and study of short-lived isomers can be found in [18, 19]. The set-up of the experiment is shown in figure 2. The LOHENGRIN mass spectrometer at ILL is used to separate the FFs recoiling from thin targets of about 400 μg cm^{-2}, according to their A/Q ratios and kinetic energies. The targets are placed near the core of the reactor in a neutron flux of 5.3×10^{14} n cm^{-2} s^{-1}. The heavy FFs have a kinetic energy of about 70 MeV and the ionic charge Q is between 18 to 24, depending on the atomic number Z. The FFs are selected by a combination of a magnetic and an electric sector field whose deflections are perpendicular to each other. At the exit of these two fields the beam is focussed by a second magnet which gives a spot of about 1×4 cm^2 area.

The FFs are detected by a ΔE gas detector of 13 cm length and subsequently stopped in a Mylar foil, 12 μm thick. The γ-rays de-exciting the isomeric states are detected by two large-volume Ge detectors and the conversion electrons are detected by two cooled adjacent

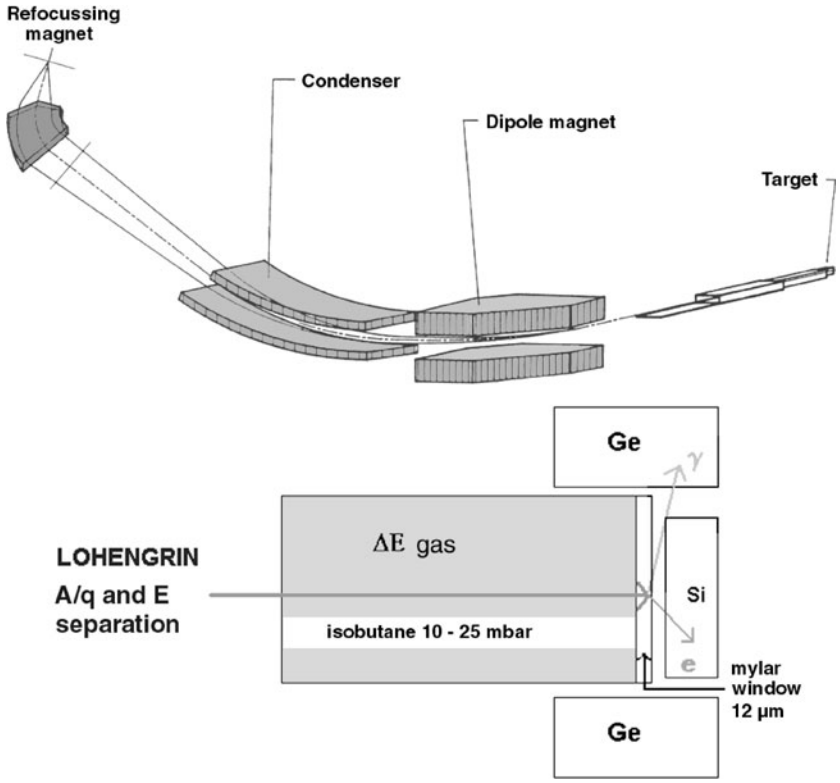

Figure 2. Schematic representation of the LOHENGRIN recoil spectrometer and the γ and conversion electron set-up placed at the focal plan of the refocussing magnet.

Si(Li) detectors covering a total area of $2 \times 6\ \mathrm{cm}^2$ and located 7 mm behind the Mylar window. The electron detection efficiency is very high, about 30%. The gas pressure of the ionization chamber is tuned to stop the FFs at about 2 μm from the outer surface of the Mylar window to minimize electron absorption and to have a good energy resolution. With this set-up, it is possible to detect conversion electrons down to about 15 keV. Note that a very low energy detection threshold and a very high detection efficiency are absolutely necessary to observe the very low energy isomeric transitions expected in nuclei close to doubly magic systems.

The distance between the source and the detectors is 23 m and the transport time through the LOHENGRIN spectrometer is about 2.2 μs, which limits the observation of isomers with half-lives longer than 0.5 μs. An event is stored on a disk, each time a Si(Li)- or a Ge-detector is fired within a time range of 40 μs after the detection of a FF.

The γ-spectrum of the microsecond isomers observed in delayed coincidence with the FFs of the $A = 129$ mass chain [20] are shown in figure 3. The observed lines belong to the microsecond isomers in the ^{129}In and ^{129}Sn isobars. The Si(Li) spectrum in coincidence with the γ-rays of ^{129}Sn [21] is also shown on the same figure. The observed lines are interpreted as the L-conversion electrons of the 19.7 and 41.0 keV isomeric transitions, respectively, while the x-rays are characteristic of the Sn isotopes and allow the atomic number identification, which is not achieved with the LOHENGRIN spectrometer. It is interesting to note that the isomeric transitions have very low energies, which is a strong characteristic of the isomers of the ^{132}Sn region.

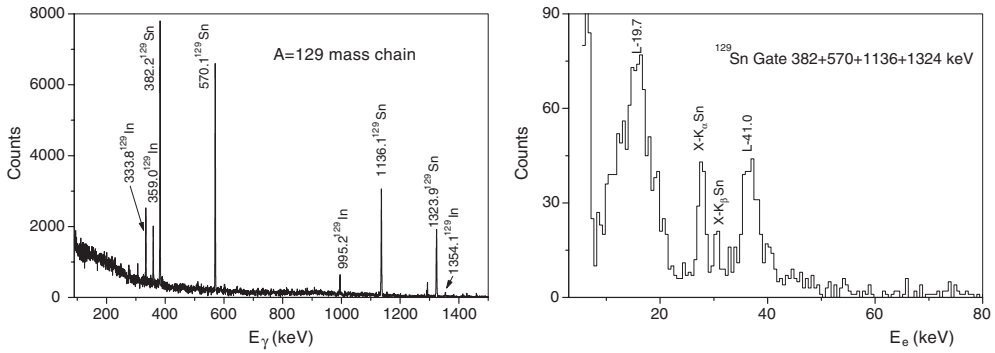

Figure 3. γ-ray spectrum of ^{129}In and ^{129}Sn isomers in delayed coincidence with FFs of $A = 129$ mass chain (left) [20]. Si(Li) spectrum in coincidence with γ-rays of ^{129}Sn (right) [21].

Zn 70	Zn 71	Zn 72	Zn 73	Zn 74	Zn 75	Zn 76	Zn 77	Zn 78 0.319 μs	Zn 79	Zn 80
Cu 69 0.36 μs	Cu 70	Cu 71 0.275 μs	Cu 72 1.76 μs	Cu 73	Cu 74	Cu 75	Cu 76	Cu 77	Cu 78	Cu 79
Ni 68 0.34 μs 0.860 μs	Ni 69 0.439 μs	Ni 70 0.21 μs	Ni 71	Ni 72	Ni 73	Ni 74	Ni 75	Ni 76 0.240 μs	Ni 77	Ni 78
Co 67	Co 68	Co 69	Co 70	Co 71	Co 72	Co 73	Co 74	Co 75	Co 76	Co 77

Figure 4. Part of the chart of nuclei showing the measured microsecond isomers in the vicinity of ^{78}Ni. The grey square corresponds to the last stable nucleus.

3. Experimental results

3.1. Microsecond isomers in the Ni region

The microsecond isomers beyond ^{68}Ni were produced by fragmentation reactions at GANIL [22, 23] with intermediate energy heavy-ion beams. They are mainly localized in the Ni and Cu isotopes close to ^{68}Ni (figure 4). It is interesting to note that no microsecond isomers were found for the Ni isotopes in the mass range $A = 71$–75, while an isomer was recently observed in ^{76}Ni [24, 25]. This unusual behaviour is discussed in detail in section 4.1.

The most interesting isomers and their leading configurations are reported in figure 5. The isomers in the even–even ^{70}Ni and ^{78}Zn decay via a cascade of four consecutive γ-rays which strongly suggests that they have a $\pi(g_{9/2})^n_{8^+}$ shell-model configuration. In the odd ^{69}Ni and ^{71}Cu the same 8^+ configuration is coupled to the neutron $\nu p_{1/2}$ or the proton $\pi p_{3/2}$, respectively.

3.2. Microsecond isomers in the Sn region

The microsecond isomers in the vicinity of ^{132}Sn were mainly produced by fission processes for the most neutron-rich nuclei or by deep inelastic reactions for the moderately neutron-rich nuclei. They are mainly localized in Sn and Sb and rapidly disappear above these isotopes (figure 6). These isomers are mainly high-spin yrast traps which decay to states which are close

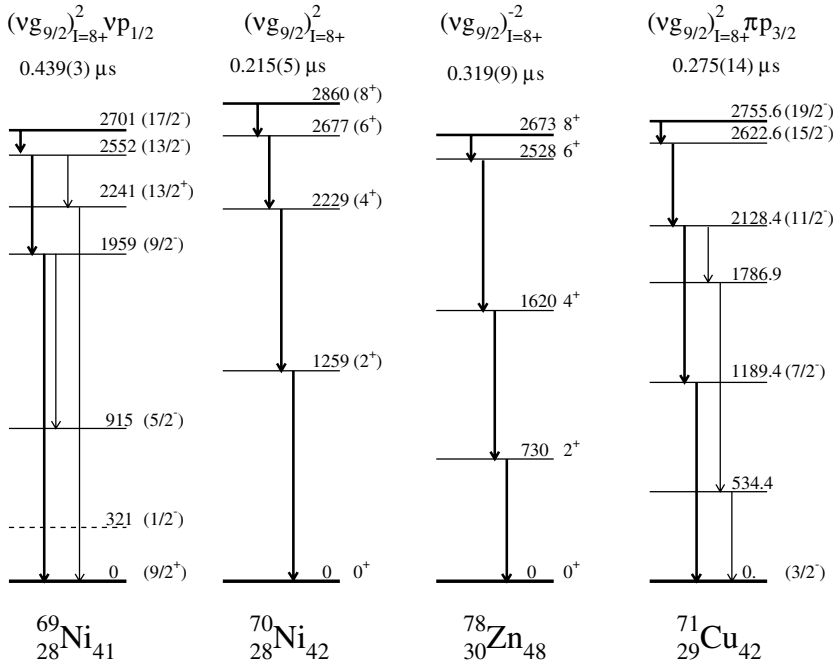

Figure 5. Experimental decay schemes of microsecond isomers in the even–even ^{70}Ni and ^{78}Zn, and in odd ^{69}Ni and ^{71}Cu. The leading structure of the microsecond isomers is also reported (from [22, 23]).

Te 125	Te 126	Te 127	Te128 0.37 µs	Te129	Te 130 1.9 µs	Te 131	Te 132 3.7 µs 28 µs	Te 133	Te 134	Te 135 0.51 µs	Te 136	Te 137
Sb 124	Sb 125	Sb 126	Sb 127 11 µs	Sb 128	Sb 129 1.1 µs	Sb 130	Sb 131 1.1 µs 4.3 µs 65 µs	Sb 132	Sb 133 17 µs	Sb 134	Sb 135	Sb 136 0.57 µs
Sn 123 34 µs 6 µs 8 µs	Sn 124 45 µs 3.1 µs 0.27 µs	Sn 125 0.23 µs 6.2 µs	Sn 126 7.6 µs 6.6 µs 10.8ns	Sn 127 4.5 µs	Sn 128 3.4 µs	Sn 129 2.4 µs 3.6 µs	Sn 130 1.61 µs	Sn 131 0.300 µs	Sn 132 2.0 µs	Sn 133	Sn 134 0.08 µs	Sn 135
In 122	In 123	In 124	In 125 9.4 µs	In 126	In 127	In 128 >10 µs	In 129 8.5 µs	In 130	In 131	In 132	In 133	In 134

Figure 6. Part of the chart of nuclei showing the measured microsecond isomers in the vicinity of ^{132}Sn. The grey squares correspond to stable nuclei.

to the yrast line. The isomeric transitions have generally very low energies and are strongly converted. These new data complete the high-spin part of the previous results obtained in β-decay experiments, where mainly low-spin levels were fed.

3.2.1. In isotopes. The nuclear structure information on the heavy In isotopes close to ^{132}Sn is very scarce. For nuclei above ^{129}In, only the ground states and long-lived isomers, decaying by β-emission, are known. High-spin millisecond and microsecond isomers were recently reported in the odd ^{125}In and ^{129}In isotopes [5] and their decay schemes are shown in figure 7. In ^{129}In, the $17/2^-$ isomer of 8.5 μs half-life [20] is assigned to the the leading $\pi g_{9/2}^{-1}\left(\nu h_{11/2}^{-1} d_{3/2}^{-1}\right)$

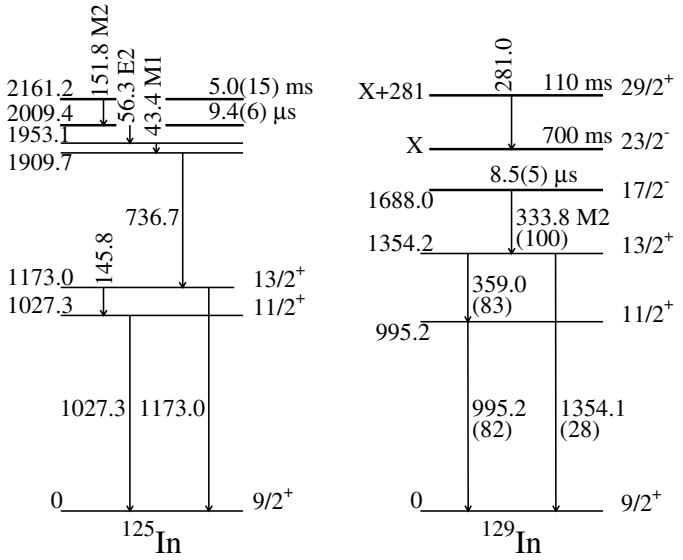

Figure 7. Experimental decay schemes of microsecond and millisecond isomers in the odd ^{125,129}In nuclei (from [5, 20]).

configuration. The $23/2^-$ and $29/2^+$ of half-life 700 and 110 ms, respectively, were tentatively assigned by Fogelberg *et al* to the fully aligned configurations $\left(\pi g_{9/2}^{-1}\nu\left(h_{11/2}^{-1}d_{3/2}^{-1}\right)\right)_{23/2^-}$ and $\left(\pi g_{9/2}^{-1}\nu h_{11/2}^{-2}\right)_{29/2^+}$, respectively. The absolute energy of the $23/2^-$ isomer which decays by β-emission is still unknown.

In ^{125}In, a 5.0 ms isomer was also observed by Fogelberg *et al* [5]. It decays by an $M2$ transition to a 9.4 μs isomer, which is de-excited by a γ-ray cascade leading to the previously known levels of 1027.3, 1173.0 and 1909.7 keV [26]. A spin and parity $I^\pi = 23/2^-$ was tentatively assigned to the excited state at 2161.2 keV by analogy with the ^{129}In nucleus. However, a spin and parity assignment $I^\pi = 25/2^+$ is also possible.

3.2.2. Sn isotopes. The systematics of the even–even Sn isotopes [1, 9, 12, 27–29] are reported in figure 8. The 10^+ microsecond isomers of leading configuration $\nu(h_{11/2})^n$ and seniority $\nu = 2$ are known in the mass range $A = 116$–130. The 7^- microsecond isomers of leading configuration $\nu(h_{11/2}d_{3/2})$ decay by an $E2$ transition to a 5^- level in the mass range $A = 118$–126. In contrast, in ^{128}Sn and ^{130}Sn, where the 5^- is above the 7^- level, the half-lives are much longer. The 5^- state is a microsecond isomer in ^{116}Sn and ^{124}Sn only.

The 8^+ isomer of 2 μs half-life in the doubly magic nucleus ^{132}Sn was first measured by Lauppe *et al* [30] at the JOSEF fission product recoil spectrometer. This high-energy state of 4848 keV energy is interpreted as a neutron-core excitation of $\left(\nu f_{7/2}h_{11/2}^{-1}\right)_{8^+}$ as a dominant configuration [31].

The ^{134}Sn nucleus [6, 32] was also added to the systematics of the even Sn although no microsecond isomer was identified in this nucleus. It is of special interest because it is the heaviest even Sn which for substantial spectroscopic information there is, and it is interesting to compare its level scheme with that of other Sn nuclei below ^{132}Sn.

The systematics of the odd Sn isotopes [10, 12, 18, 21] are reported in figure 9. The $27/2^-$ microsecond isomers of the dominant configuration $\nu(h_{11/2})^n$ and seniority $\nu = 3$ are known in the mass range $A = 119$–125. The half-life of this isomer is most likely too short

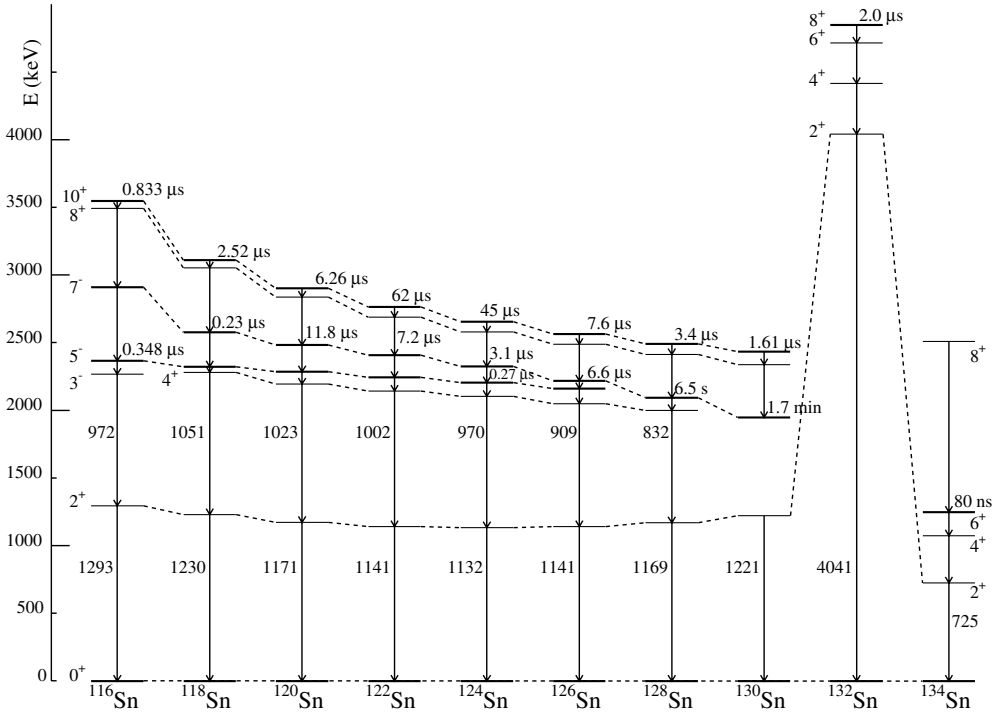

Figure 8. Experimental decay schemes of microsecond isomers in the even Sn nuclei and in ^{134}Sn which has an isomer of 80 ns half-life.

to be measured in ^{127}Sn and ^{129}Sn with the LOHENGRIN recoil spectrometer, where the time of flight of the FFs through the spectrometer is about 2 μs.

The $23/2^+$ and $19/2^+$ microsecond isomers of the dominant configuration $\nu\left(h_{11/2}^{-2}d_{3/2}^{-1}\right)$ are also observed, but while the latter is known in the mass range $A = 119$–129, the former is known only in ^{123}Sn and ^{129}Sn.

3.2.3. Sb isotopes. Microsecond isomers are known in the four odd $^{127-133}$ Sb isotopes [3, 19, 20, 33]. The three Sb nuclei below ^{132}Sn are reported in figure 10. Several isomers are present in ^{129}Sb and ^{131}Sb isotopes. The main difference between these two nuclei is the inversion of the $15/2^-$ and $19/2^-$ states. The consequences of this feature are dramatic for the $19/2^-$ state that has a different half-life in these two nuclei: in ^{131}Sb it decays by an $E2$ transition and its half-life is 4.3 μs, while in ^{129}Sb it decays by an $M4$ transition or a β-emission and its half-life is 17.7 min. The dominant configuration of the positive parity $23/2^+$ microsecond isomers is $\pi g_{7/2}\nu h_{11/2}^{-2}$, while for the negative parity $15/2^-$ and $19/2^-$ isomers it is $\pi g_{7/2}\nu\left(d_{3/2}^{-1}h_{11/2}^{-1}\right)$.

The nucleus ^{133}Sb consists of the doubly magic ^{132}Sn plus one valence proton. This nucleus was studied simultaneously with the LOHENGRIN spectrometer [33] and with the multidetector EUROGAM2 [34] using a spontaneously fissioning ^{248}Cm source. These two complementary works, where conversion electrons, angular correlations and linear polarization were measured have allowed the level scheme of figure 11 to be constructed, where all the spins and parities are unambiguously assigned. The conversion electrons of the isomeric transition were not observed with the Si(Li) detector of the LOHENGRIN experiment. This

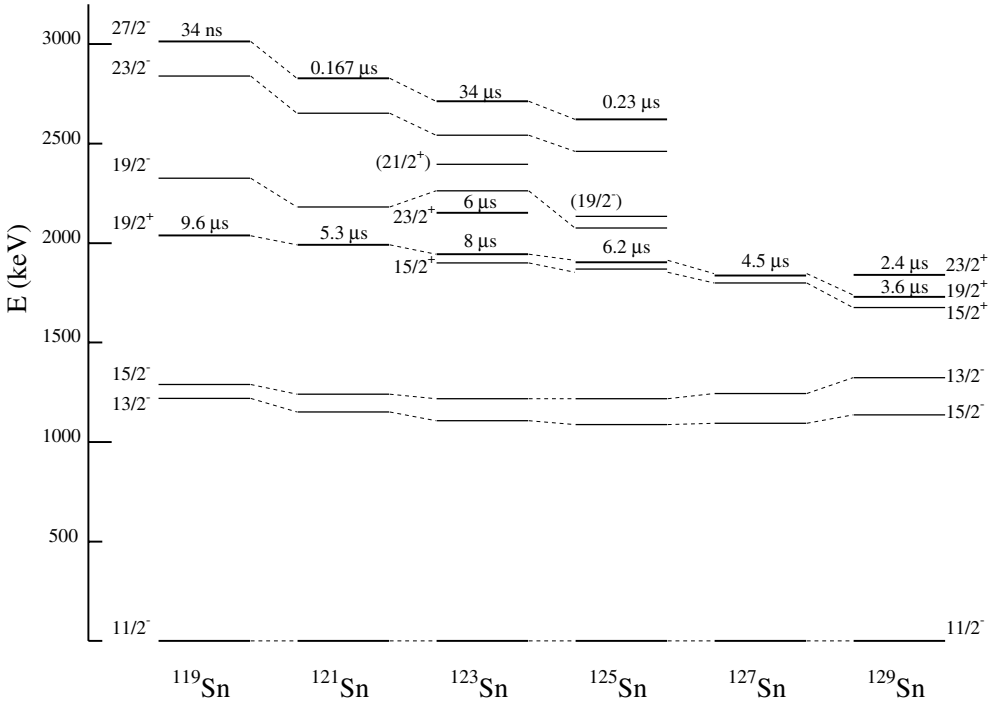

Figure 9. Experimental levels of the odd Sn nuclei fed by the decay of microsecond isomers.

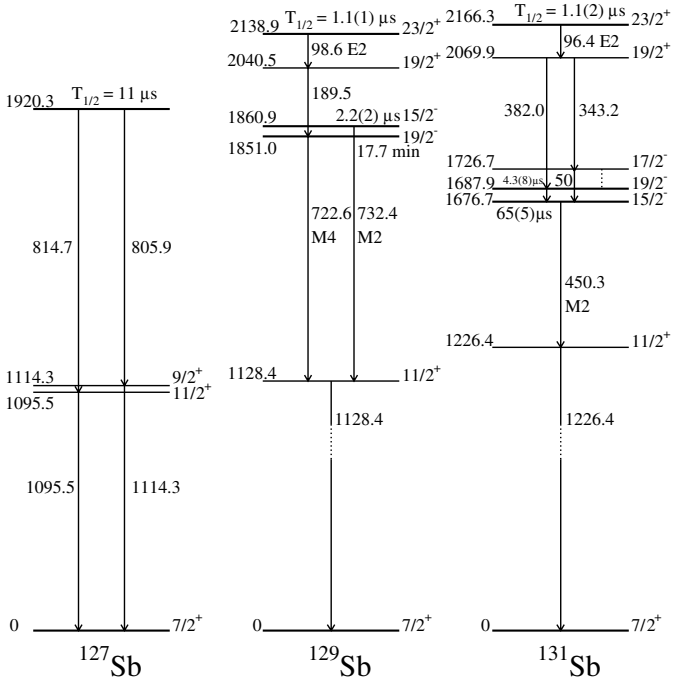

Figure 10. Experimental decay schemes of microsecond isomers in the odd ^{127,129,131}Sb nuclei (from [3, 19, 20]).

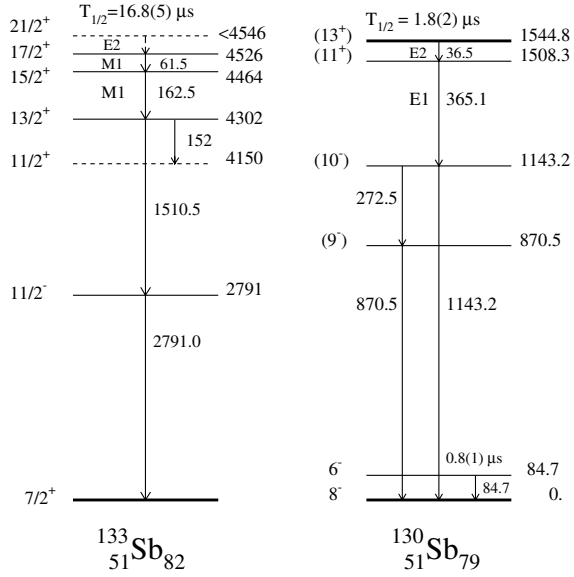

Figure 11. Experimental decay schemes of microsecond isomers in the ^{133}Sb [33] and ^{130}Sb [21] nuclei.

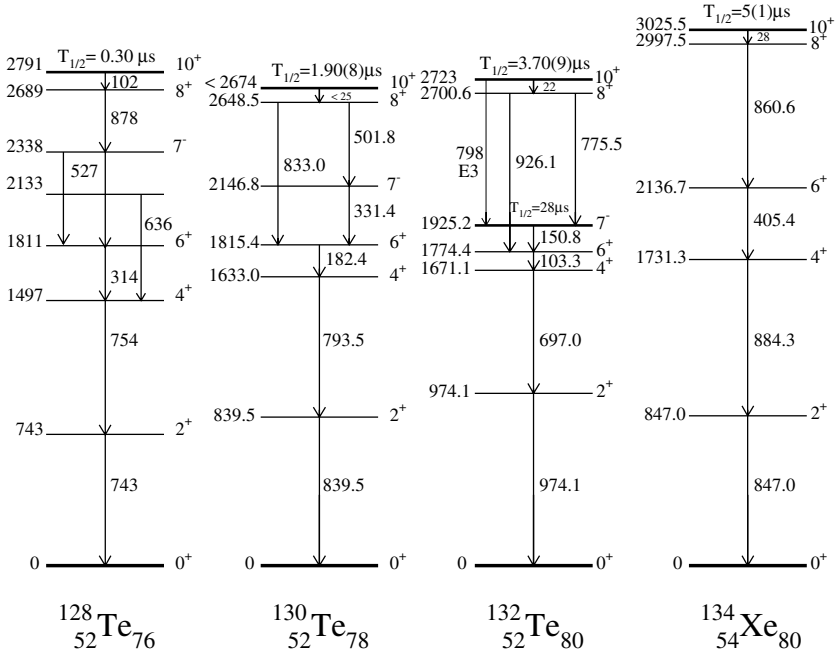

Figure 12. Experimental decay schemes of microsecond isomers in even–even ^{128,130,132}Te and ^{134}Xe [13, 35].

feature requires that its energy should be lower than 20 keV. The $21/2^+$ isomeric state has the dominant $\pi g_{7/2}\nu\left(f_{7/2}h_{11/2}^{-1}\right)$ core excitation configuration.

Table 1. Leading configurations of the measured microsecond isomers.

Nuclei	Spin and parity	Shell-model configuration
^{70}Ni, ^{78}Zn	8^+	$\nu g_{9/2}^n$, $\nu = 2$
^{69}Ni	$17/2^-$	$\nu\left(g_{9/2}^2 p_{1/2}^{-1}\right)$
^{69}Cu	$13/2^+$	$\pi p_{3/2} \nu\left(p_{1/2}^{-1} g_{9/2}\right)$
^{71}Cu	$19/2^-$	$\nu g_{9/2}^2 \pi p_{3/2}$
^{125}In	$17/2^-$	$\pi g_{9/2}^{-1} \nu\left(h_{11/2}^{-1} d_{3/2}^{-1}\right)$
^{128}In	(1^-)	$\pi p_{1/2}^{-1} \nu d_{3/2}^{-1}$
^{116}Sn–^{130}Sn	10^+	$\nu h_{11/2}^n$, $\nu = 2$
^{119}Sn–^{125}Sn	$27/2^-$	$\nu h_{11/2}^n$, $\nu = 3$
^{118}Sn–^{126}Sn	7^-	$\nu(h_{11/2} d_{3/2})$
^{123}Sn, ^{129}Sn	$23/2^+$	$\nu\left(h_{11/2}^2 d_{3/2}\right)$
^{123}Sn–^{129}Sn	$19/2^+$	$\nu\left(h_{11/2}^2 d_{3/2}\right)$
^{132}Sn	8^+	$\nu\left(h_{11/2}^{-1} f_{7/2}\right)$
^{129}Sb, ^{131}Sb	$23/2^+$	$\pi g_{7/2} \nu h_{11/2}^{-2}$
^{129}Sb	$15/2^-$	$\pi g_{7/2} \nu\left(h_{11/2}^{-1} d_{3/2}^{-1}\right)$
^{131}Sb	$19/2^-$	$\pi g_{7/2} \nu\left(h_{11/2}^{-1} d_{3/2}^{-1}\right)$
^{130}Sb	13^+	$\pi g_{7/2} \nu\left(h_{11/2}^{-2} d_{3/2}^{-1}\right)$
^{133}Sb	$21/2^+$	$\pi g_{7/2} \nu\left(h_{11/2}^{-1} f_{7/2}\right)$

3.2.4. Even–even Te and Xe isotopes. Recently, the microsecond isomers in the even–even ^{130,132}Te and ^{134}Xe isotopes were investigated with the LOHENGRIN spectrometer [35]. In these experiments the $10^+ \rightarrow 8^+$ isomeric transitions of ^{132}Te and ^{134}Xe were measured for the first time. Very low energies of 22 and 28 keV were respectively found. In ^{130}Te the isomeric transition was not observed, which requires a conservative upper limit of its energy of $E \sim 25$ keV. The level schemes of these three isomers and ^{128}Te produced by deep-inelastic reactions [6] are reported in figure 12. These isomers are analogous to the ones already observed in the even Sn isotopes and have the dominant $\nu h_{11/2}^{-2}$ configuration.

3.2.5. Odd–odd nuclei. Very few microsecond isomers were observed in the odd–odd nuclei in the vicinity of ^{132}Sn. Three isomers are reported in the literature in ^{128}In [4], ^{130}Sb [21] and ^{136}Sb [17]. In ^{128}In only a lower limit of the half-life $T_{1/2} > 10$ μs is known [4]. The most interesting is the ^{130}Sb nucleus, where an $I^\pi = 13^+$ isomer, arising from the $\pi g_{7/2} \nu\left(d_{3/2}^{-1} h_{11/2}^{-2}\right)$ configuration, was observed and is reported in figure 11. These data complete a previous β-decay experiment of Walters and Stone [36] and several members of different proton-particle neutron-hole multiplets were identified. This nuclear structure information is of fundamental importance to test the neutron–proton interaction in this region, as is discussed in more detail in section 4.2.2.

The spins of the isomers and their leading configurations are reported in table 1.

4. Comparison with shell-model calculations

Spectroscopic studies around doubly magic nuclei with large N/Z ratio provide an excellent probe of shell structure and effective interactions. Empirical and realistic two-body matrix

elements have been used in these calculations. While the empirical shell-model calculations are quite successful in describing the nuclear structure properties, they are not satisfactory in that the fundamental goal of nuclear structure theory is to understand the properties of complex nuclei in terms of the nucleon–nucleon (N–N) interaction. Since the pioneering work of Kuo and Brown [37] there has been considerable progress towards a microscopic approach to nuclear structure calculations starting from the free N–N potential. In these realistic models, only the effective two-body matrix elements are computed. Moreover, as the single-particle states are not correctly reproduced by the theory, their experimental values are used in the calculations. They are generally well known in the vicinity of ^{132}Sn, but still unknown in the vicinity of ^{78}Ni. Recently, large shell model calculations were developed, which enables a detailed comparison not only of level schemes, but also of electromagnetic transition rates.

4.1. Shell model in the ^{78}Ni region.

The structure of the microsecond isomers beyond the semi-magic ^{68}Ni nucleus is expected to be governed by the filling of the $\nu g_{9/2}$ orbital. In fact, the $\nu(g_{9/2})^n_{8^+}$ configuration isomers were experimentally observed in the even–even nuclei ^{70}Ni (with two neutron particles) and ^{78}Zn (with two neutron holes) [22, 23]. It was also identified in the microsecond isomers of the odd neighbouring nuclei, $^{69}_{28}\mathrm{Ni}_{41}$ and $^{71}_{29}\mathrm{Cu}_{42}$, where it is coupled to the neutron $\nu p_{1/2}$ and proton $\pi p_{3/2}$, respectively [22].

Surprisingly, the $\nu(g_{9/2})^n_{8^+}$ isomers were not found in the more neutron-rich ^{72}Ni and ^{74}Ni. More precisely, these isomers could be excluded from the half-life range 20 ns $< T_{1/2} <$ 2.5 ms for ^{72}Ni and 60 ns $< T_{1/2} <$ 0.2 ms for ^{74}Ni [24]. These experimental findings are at variance with the experimental data in other magic regions where an isomeric transition takes place between the two highest spin states of the j^n and $\nu = 2$ or 3 seniority configurations. Such isomers were already found for the $\pi g_{9/2}$ ($N = 50$), $\pi h_{11/2}$ ($N = 82$), $\pi h_{9/2}$ ($N = 126$), $\nu h_{11/2}$ ($Z = 50$) and $\nu i_{13/2}$ ($Z = 82$) orbitals [38].

To shed some light on this puzzle, a shell-model calculation was performed by Grawe *et al* [39] by using the full $\pi\nu(p_{1/2}, p_{3/2}, f_{5/2}, g_{9/2})$ model space and the realistic two-body matrix elements were obtained from the S3V interaction of Sinatkas *et al* [40]. For details of the calculations see [39, 41]. The $I^\pi = 8^+$ isomers in ^{70}Ni and ^{78}Zn are well reproduced by the theory, as well as the $I^\pi = 17/2^-$ in ^{69}Ni and $I^\pi = 19/2^-$ in ^{71}Cu. The $B(E2)$ transition probabilities are also well reproduced using effective charges $e_\nu = 1.0\,e$ and $e_\pi = 1.5\,e$. The comparison between the experimental data and theory for ^{70}Ni, ^{78}Zn and ^{69}Ni is shown in figure 13.

The same calculation was also performed for ^{72}Ni and is compared in figure 14 with the experimental level scheme of this nucleus measured from the β-decay of ^{72}Co [42]. This computation predicts a very small $B(E2)$ value for the $8^+ \rightarrow 6^+$ transition in ^{72}Ni. This would result in an isomeric half-life of about 20 μs, which is well within the experimental sensitivity. This $B(E2)$ quenching is a consequence of the $\nu g_{9/2}$ subshell filling and a deep minimum is expected for the $E2$ transition rate at the mid-subshell occupation. An effect of this nature is observed for instance for the $\nu h_{11/2}$ neutron subshell in the even- and odd-mass Sn isotopes (see section 5 and figure 21(A)).

In the previous realistic calculation, the lowest 6^+_1 level has the seniority $\nu = 2$, while a second 6^+_2 of seniority $\nu = 4$ is above the 8^+ state. However, another calculation performed by Grawe *et al* [39] has shown that the situation could be reversed in ^{72}Ni. Using an empirical approach, where the $\nu(g_{9/2})^2$ two-body matrix elements were the experimental energies of ^{70}Ni, levels with seniority $\nu = 4$ were calculated. It turned out that the $I^\pi = 6^+_1$, $\nu = 4$ state

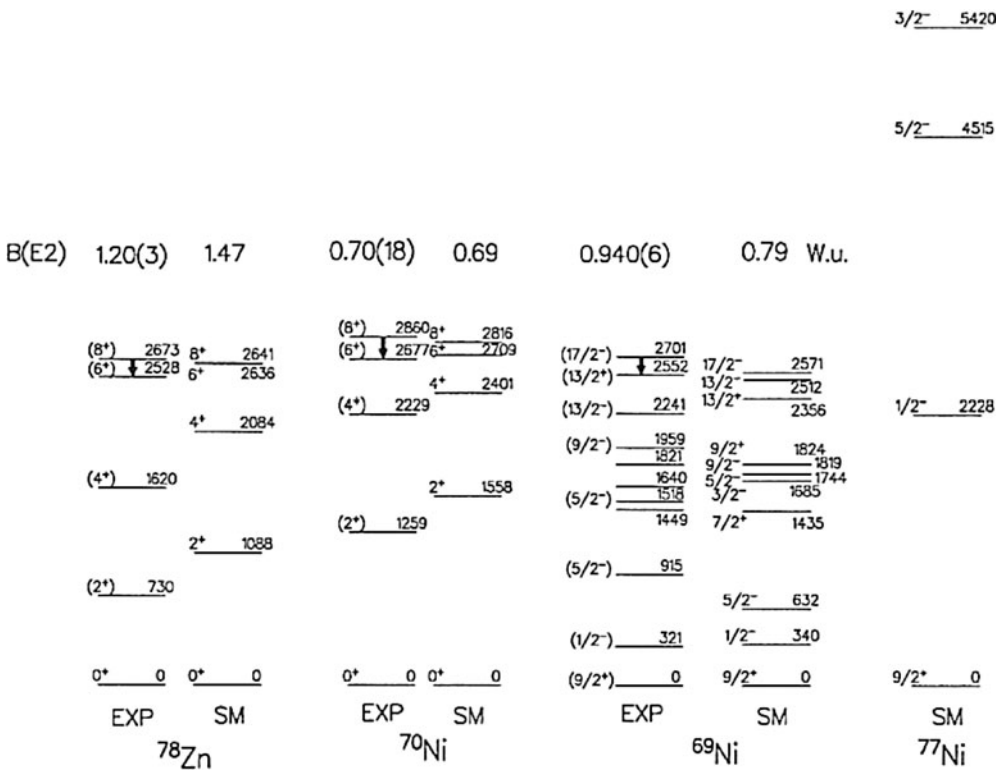

Figure 13. Experimental and calculated decay schemes of the $I^{\pi} = 8^{+}$ in ^{70}Ni and ^{78}Zn, and the $I^{\pi} = 17/2^{-}$ in ^{69}Ni. The shell model extrapolation to one-neutron hole nucleus in ^{77}Ni is also shown (from [39]).

should be somewhat lower than the $I^{\pi} = 8^{+}, \nu = 2$ level (see figure 14). This would lead to a fast $\left(B(E2); 8^{+} \rightarrow 6_{2}^{+}\right), \Delta\nu = 2$ transition, resulting in a predicted half-life of about 20 ns, whereas 20 μs are expected in the S3V shell model. The half-life predicted by the empirical shell model is too short to be measured by the LISE3 spectrometer. The inversion effect between the $\nu = 2$ and $\nu = 4$ seniority states is very rare in the chart of nuclei and was only known in the neutron and proton $f_{7/2}$ ($N = 28$) orbitals [38]. In figure 14 one can see that the energy of the 2_{1}^{+} level in ^{72}Ni, which was computed with the S3V realistic interaction, has a much higher energy than the experimental value. This effect, which is most likely the consequence of too limited model space used in the calculations, might induce the observed seniority inversion.

If the above interpretation is correct, the isomerism which is expected to disappear in ^{72}Ni and ^{74}Ni, should reappear towards the end of the $\nu g_{9/2}$ shell for ^{76}Ni, because only the excited states with seniority $\nu = 2$ should be observed. A new study of the neutron-rich Ni isotopes was performed very recently at GANIL. Two γ-rays of 144 and 930 keV were assigned to a 240 (80) ns isomer in ^{76}Ni [24, 25]. However, this result is still puzzling because only two of the four expected transitions de-exciting the $\nu g_{9/2}^{-2}$ configuration were observed. Consequently, although a microsecond isomer was observed in this nucleus, it is not possible to identify it unambiguously with the 8^{+} level. Better experimental statistics are required to clarify the structure of the heavy Ni nuclei.

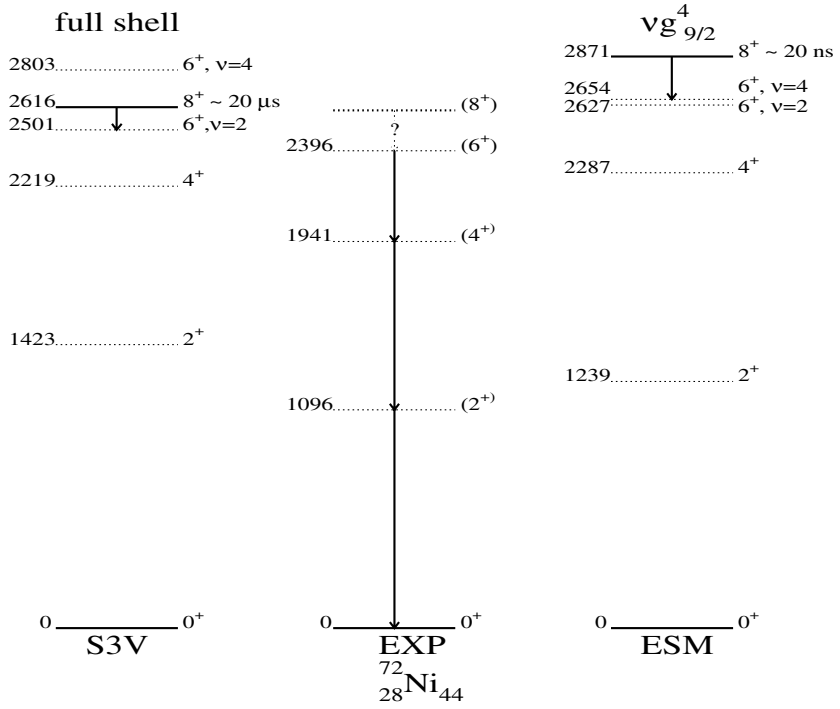

Figure 14. Comparison of the experimental level scheme of ^{72}Ni with a realistic calculation (S3V) and an empirical calculation (ESM). Different behaviour is observed for the two 6^+ levels in the two models (from [42]).

4.2. Shell model in the ^{132}Sn region

At present, the experimental nuclear-structure information available for the ^{132}Sn region is more abundant than for the ^{78}Ni region, which is much further from the stability line. The new data recently obtained from the decay of microsecond isomers have considerably extended our experimental knowledge of the heavy Sn and Sb isotopes especially at high spins. They offer the opportunity for testing the ingredients of shell-model calculations in very neutron-rich nuclei which also have very strong shell closures for both neutrons and protons. Empirical and realistic shell-model calculations are available in the ^{132}Sn region.

4.2.1. Empirical calculations. Insolia *et al* [43] have studied the odd- and even-Sn isotopes in the framework of a multistep shell-model formalism, using for the two-body matrix elements the extrapolated values of the two-particle experimental data measured in ^{206}Pb. The one- to four-quasi-particle states were computed with this model in the mass range $A = 114$–131. Comparing experimental values of figure 15 with the corresponding calculations one can say that the agreement is good, although a deterioration is observed towards the semi-magic number $N = 64$. This feature is a manifestation of the the breakdown of the BCS approximation near $A = 114$.

It is also shown in this work that there are many components that contribute appreciably to the wavefunction of the 2^+_1 state. The $h_{11/2}$ configuration is dominant, close to $A = 130$, but its importance gradually decreases as one approaches $A = 114$. Instead, the 4^+_1 and the

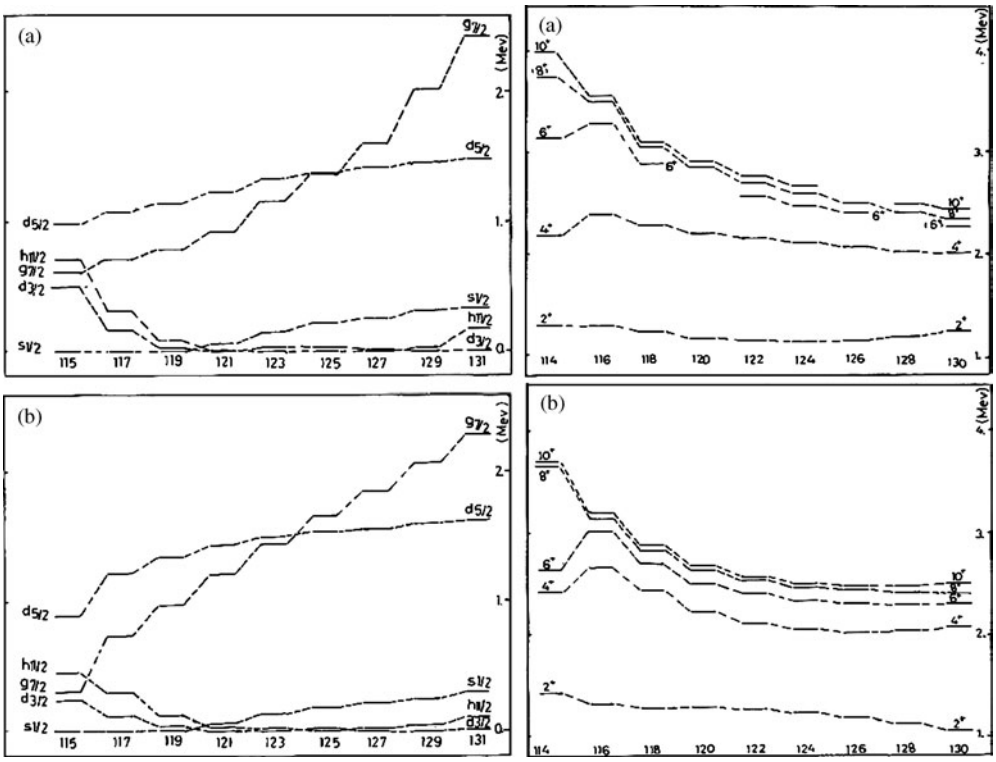

Figure 15. Experimental (a) and calculated (b) one- and two-particle energies in Sn nuclei as a function of the mass number A (from [43]).

higher spin states up to 10^+ have an almost pure $\nu(h_{11/2})^2$ configuration all through the studied region.

Unfortunately, apart from the one-quasi-particle states, no predictions were reported for the odd nuclei above $A = 123$, because the high-spin states were still unknown when the work was published.

4.2.2. Realistic calculations. Very recently two groups have performed calculations in the ^{132}Sn region, using realistic two-body matrix elements derived from realistic N–N potentials.

Holt *et al* [44] calculated the low-lying spectra of the Sn isotopes in the mass range $A =$ 120–130. Unfortunately, the high-spin states in the heavy odd Sn isotopes were still unknown when this work was published and the paper focussed attention on the low-spin states.

A more complete theoretical work was recently carried out by the Napoli group which performed shell-model calculations for several nuclei close to ^{132}Sn [45–48, 20] using the Bonn-A and CD-Bonn N–N potentials. This model was previously tested, with success, in the ^{208}Pb region [49].

In these calculations the doubly-magic ^{132}Sn is considered as a closed core. The single-particle and single-hole energies used in the calculations and reported in table 2 are taken from the experimental spectra of ^{133}Sb, ^{131}Sn and ^{131}In semi-magic nuclei, respectively. Some of these states are still unknown. As regards the neutron-hole energies, the experimental value proposed by Fogelberg and Blomqvist [50] for the $\nu 0h_{11/2}^{-1}$ level is most likely wrong and the calculated energy of 0.100 MeV suggested in [33] is adopted in the calculations.

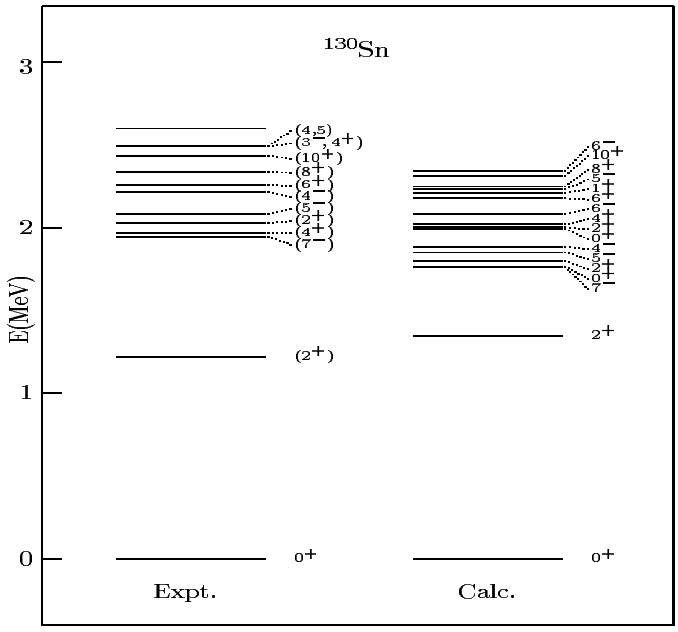

Figure 16. Experimental and calculated spectrum of ^{130}Sn [45].

Table 2. Single-particle and single-hole energies ϵ (MeV) adopted in the calculations [20].

Neutron-hole level	ϵ	Proton-particle level	ϵ	Proton-hole level	ϵ
$1d_{3/2}$	0.000	$0g_{7/2}$	0.000	$1g_{9/2}$	0.000
$0h_{11/2}$	0.100	$1d_{5/2}$	0.962	$1p_{1/2}$	0.365
$2s_{1/2}$	0.332	$1d_{3/2}$	2.439	$1p_{3/2}$	1.650
$1d_{5/2}$	1.655	$0h_{11/2}$	2.793	$0f_{5/2}$	2.750
$0g_{7/2}$	2.434	$1s_{1/2}$	2.800		

The experimental energy of the $\pi 2s_{1/2}$ level is unknown and its position was determined at 2.8 MeV by reproducing the experimental energy of the $1/2^+$ level at 2.15 MeV in ^{137}Cs. The energies of the $\pi(1p_{1/2}, 1p_{3/2}, 0f_{5/2})$ levels, reported by Hannawald *et al* [51], correspond to a tentative assignment from γ-rays measured in the β-decay of ^{131}Cd.

The simplest systems to study are the nuclei having two identical valence particles or holes outside the ^{132}Sn core, such as ^{130}Sn or ^{134}Te. All the experimental and calculated levels of ^{130}Sn, up to about 2.5 MeV, are reported in figure 16. It should be noted that above this excitation energy there is a gap of about 0.700 MeV both in the experimental- and theoretical-level schemes. This gap reflects the gap observed in the single-hole neutron energies between the $s_{1/2}$, $d_{3/2}$, $h_{11/2}$ levels and the $d_{5/2}$, $g_{7/2}$ levels, respectively. The agreement between theory and experiment is very satisfactory. Each of the nine experimental lowest-lying excited states, except the 2_2^+, can be identified with a level predicted by the theory. The authors quote that the rms deviation divided by the number of levels (σ) is 0.175 MeV.

The experimental and calculated levels of ^{134}Te are reported in figure 17 (for a detailed discussion see [46]). The rms deviation σ relative to the states shown in figure 17 is

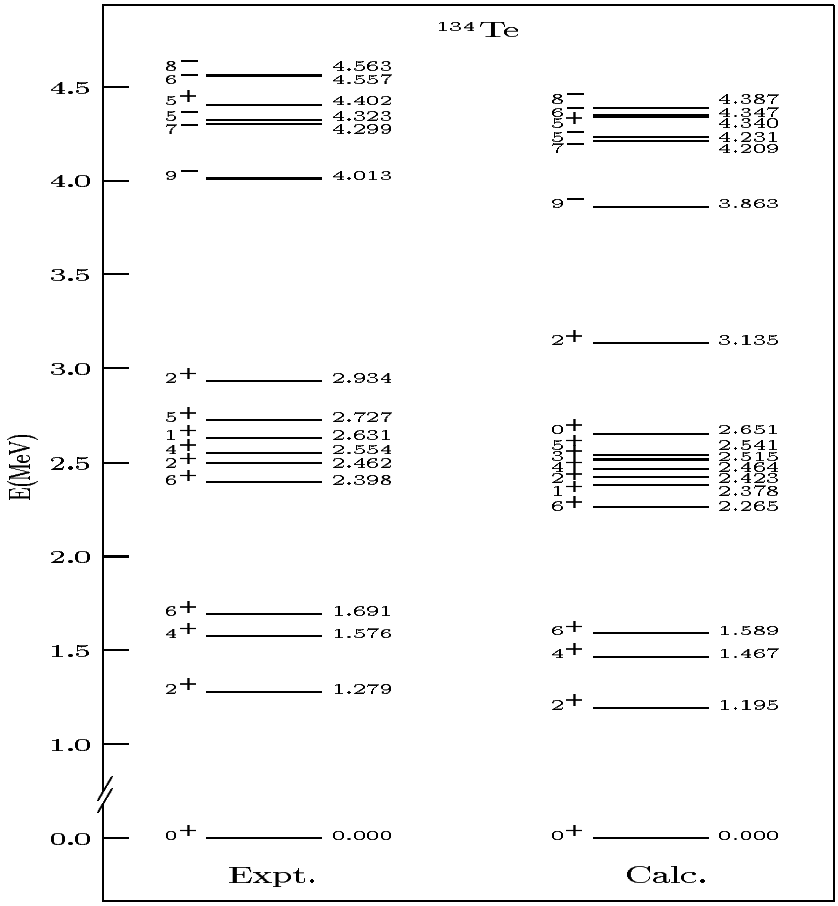

Figure 17. Experimental and calculated spectra of ^{134}Te [46].

0.145 MeV. The most important discrepancy concerns the 2_3^+ state, measured at 2.934 MeV and computed at 3.135 MeV.

The next step includes testing the realistic proton–neutron effective interactions in odd–odd nuclei. Unfortunately, the available experimental data for this kind of nucleus are still rather scarce and only ^{132}Sb [36, 52, 53] and ^{130}Sb [21, 36] with one proton particle and one and three neutron holes, respectively, have been studied. The experimental and calculated levels of ^{130}Sb, up to 1.3 MeV, are reported in figure 18, where the complementary data obtained in the decay of the 13^+ isomer and in the β-decay of ^{130}Sn have been added to the experimental level scheme. The levels belong to several multiplets of configurations $\pi g_{7/2}\nu h_{11/2}^{-1}$, $\pi g_{7/2}\nu d_{3/2}^{-1}$, $\pi g_{7/2}\nu s_{1/2}^{-1}$, with two neutron holes forming a zero-coupled pair, and $\pi g_{7/2}\nu d_{3/2}^{-1}h_{11/2}^{-2}$ are compared with the theory and the discrepancies are all of the order of a few tens of keV.

In [47] the behaviour of the proton–neutron-hole multiplets has been investigated showing that the highest- and lowest-spin members of each multiplet are well separated from the other states which lie very close in energy. This behaviour is consistent with the experimental data of the $\pi g_{7/2}\nu h_{11/2}^{-1}$ multiplet where five of the eight members were observed in ^{130}Sb and in the $\pi g_{7/2}\nu d_{3/2}^{-1}$ mutiplet in ^{130,132}Sb. Moreover, it is noteworthy that in all of the calculated

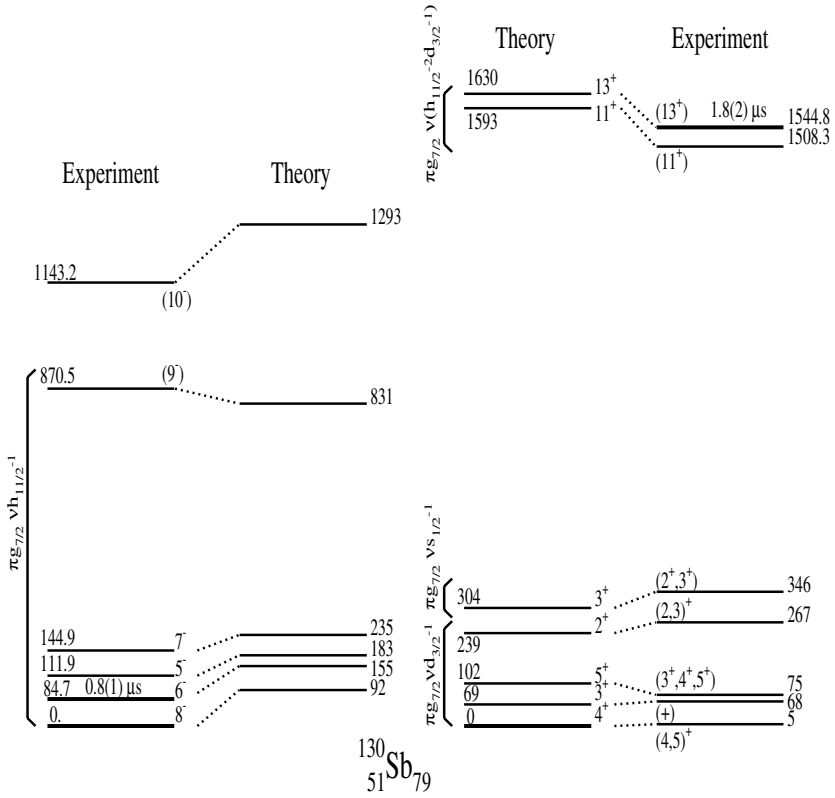

Figure 18. Experimental and calculated spectra of the odd–odd ^{130}Sb [47]. The experimental data come from the decay of the 1.8 μs isomer in ^{130}Sb [21] and from the β-decay of ^{130}Sn [36].

multiplets the state of spin $j_\pi + j_\nu - 1$ is the lowest, in agreement with the predictions of the Brennan–Bernstein coupling rule.

In figure 19 the experimental yrast levels in the odd ^{129}In, ^{129}Sb and ^{131}Sb nuclei are compared with the calculated ones. As regards the quantitative agreement, we see that the observed excitation energies are very well reproduced by the calculations. The only significant discrepancy occurs (in all three nuclei) for the $11/2^+$ state, which is predicted to lie a few hundreds keV above its experimental counterpart. In ^{129}In and ^{131}Sb the $11/2^+$ state results from the coupling of 2^+ in ^{130}Sn with a proton $\pi g_{9/2}^{-1}$ or $\pi g_{7/2}$, respectively. However, the theoretical energy of the 2^+ level is predicted with too high energy in ^{130}Sn, which most likely explains the discrepancy observed in the two odd-mass nuclei. Note that this discrepancy also leads to an inversion in the ordering of the $13/2^+$ and $11/2^+$ levels in ^{129}In.

In table 3 the experimental data [5, 19, 20] are compared with the theoretical predictions for the electromagnetic transition rates and half-lives, the latter obtained by using experimental γ-ray de-excitation energies, whenever available, and including the conversion electrons. The $E2$ transition rates in Sb isotopes have been calculated with an effective proton charge $e_\pi^{\rm eff} = 1.55e$, while for the proton hole in ^{129}In the value $e_\pi^{\rm eff} = 1.35\ e$. For the neutron hole the value of 0.78 e, which reproduces the experimental value of the $B(E2; 10^+ \rightarrow 8^+)$ in ^{130}Sn, is adopted. In the calculation of the magnetic transitions free gyromagnetic factors are used, since reasonable changes in their values would only slightly affect the final results. By

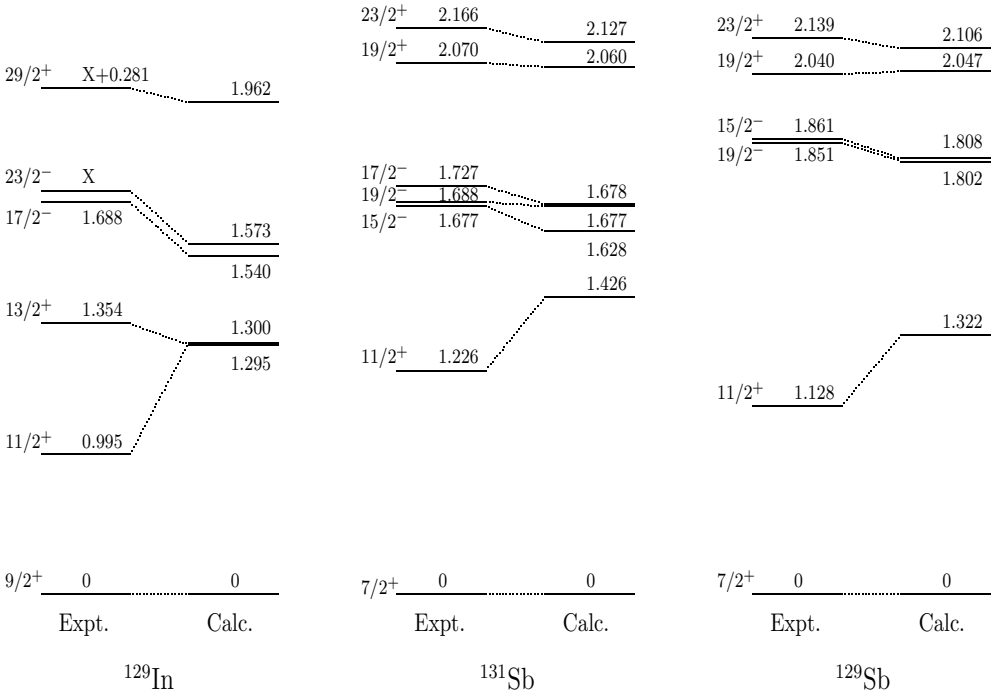

Figure 19. Experimental and calculated energy levels in ^{129}In, ^{131}Sb and ^{129}Sb. Only levels close to the yrast line and mainly fed by millisecond or microsecond isomers are reported (from [19, 20]).

Table 3. Calculated and experimental reduced transition probabilities (W.u.) in ^{131}Sb, ^{129}In and ^{129}Sb (from [20]).

			Reduced transition probability	
Nucleus	Transition	$J_i^\pi \to J_f^\pi$	Calculated	Experimental
^{131}Sb	$E2$	$23/2^+ \to 19/2^+$	0.60	0.53(10)
	$E2$	$19/2^+ \to 15/2^+$	1.02	
	$E2$	$19/2^- \to 15/2^-$	1.24	0.99(18)
	$M2$	$15/2^- \to 11/2^+$	0.33×10^{-2}	$0.66(11) \times 10^{-3}$
^{129}In	$E3$	$29/2^+ \to 23/2^-$	0.52×10^{-1}	$0.66(10) \times 10^{-1}$
	$M2$	$17/2^- \to 13/2^+$	0.45×10^{-1}	$0.32(2) \times 10^{-1}$
^{129}Sb	$E2$	$23/2^+ \to 19/2^+$	0.97	0.51(9)
	$E2$	$19/2^+ \to 15/2^+$	1.07	
	$M2$	$15/2^- \to 11/2^+$	0.25×10^{-2}	$0.26(3) \times 10^{-2}$

comparing with the experimental data in table 3, we see that quite good agreement is obtained in all the cases considered.

In conclusion, the calculated results obtained using two-body effective interactions derived from realistic N–N potentials provide a very satisfactory interpretation of the experimental spectra and electromagnetic transition rates of nuclei close to the doubly-magic ^{132}Sn. However, the last known even–even Sn nucleus, ^{134}Sn, with two neutrons outside the closed core, is characterized by a very low-energy 2^+ state at 725 keV (see figure 20). In fact, it is the

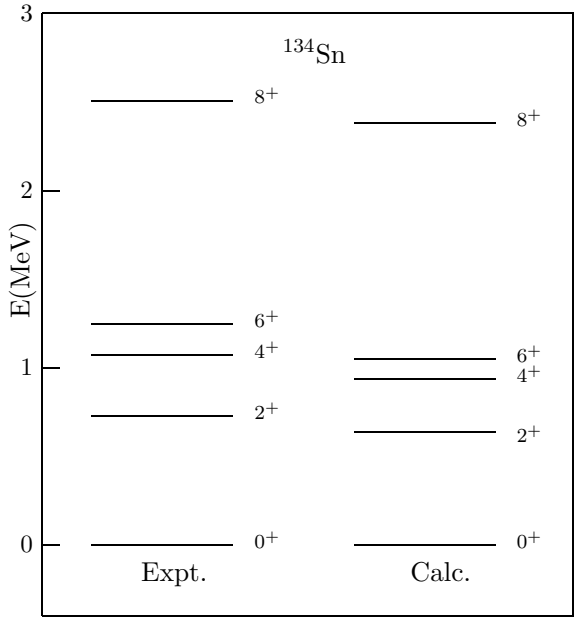

Figure 20. Experimental and calculated spectra of ^{134}Sn. The experimental 2^+ level has the lowest energy measured for an even–even semi-magic nucleus in the whole chart of nuclides (from [48]).

lowest 2_1^+ level measured for a semi-magic even–even nucleus in the whole chart of nuclides. It is, therefore, interesting to know if it may still be described in the framework of the shell model or if some collective effects are needed to explain the lowering of this 2_1^+ state. Very recently, Corraggio *et al* [48] have performed shell-model calculations for ^{134,135}Sn, using the CD-Bonn N–N potential. The experimental single-particle energies $\nu(p_{1/2}, p_{3/2}, f_{5/2}, h_{9/2})$ are used in the calculations, while the still unknown energy of the $\nu i_{13/2}$ was estimated. The calculated spectrum of ^{134}Sn in figure 20 shows that there is a very good agreement with the experimental data. The experimental 0^+, 2^+, 4^+ and 6^+ are dominated by the configuration $\nu f_{7/2}^2$, while the 8^+ by $\nu(f_{7/2}h_{9/2})$. One may conclude that no substantial departure from the shell model seems to be present in this mass region up to a high N/Z ratio of 1.68.

5. $B(E2)$ transition rates in even Sn and Te isotopes

As discussed in section 3, 10^+ microsecond isomer were identified in several even–even Sn and Te isotopes and in figure 21(A) the experimental $B(E2; 10^+ \rightarrow 8^+)$ transition rates of the isomeric transitions are plotted against neutron number [54]. A strong enhancement of the $B(E2)$ values is observed for the Te isotopes and they increase when the neutron number decreases, whereas the trend is inverted for the Sn isotopes. The origin of this enhancement is discussed by Genevey *et al* [35, 54].

In the Sn nuclei, the observed trend reflects the filling of the $\nu h_{11/2}$ neutron subshell, which shows a deep minimum for 73 neutrons, corresponding to the mid-subshell. Hence, one may conjecture that in the Te isotopes, with two valence protons outside the $Z = 50$ magic shell, this effect is completely masked by some admixture from other configurations. In fact, the most efficient way to increase the $B(E2, 10^+ \rightarrow 8^+)$ strength in the Te isotopes is to suppose that the $\{\nu(h_{11/2}^{-2}) \times \pi(0^+)\}_{8^+,10^+}$ leading components are mixed with the $\{\nu(h_{11/2}^{-2}) \times \pi(2^+)\}_{8^+,10^+}$

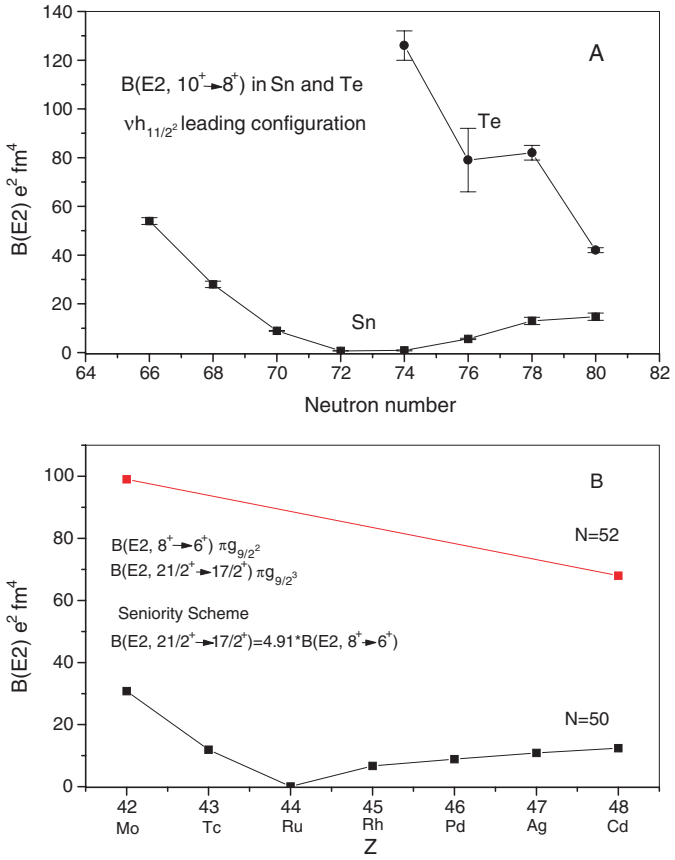

Figure 21. (A) $(B(E2), 10^+ \rightarrow 8^+)$ values in the Sn and Te isotopes. (B) $(B(E2), 8^+ \rightarrow 6^+)$ and $(B(E2), 21/2^+ \rightarrow 17/2^+)$ values in the $N = 50$ and $N = 52$ isotones (adapted from [54]). The $B(E2)$ values of the odd A nuclei are renormalized according to the seniority formula.

ones, where the proton pair is excited to a 2^+ configuration. The underlying cause of the mixing is the residual p–n interaction. Then, the transition takes place between the initial state:

$$|10^+\rangle = \{\nu(10^+) \times \pi(0^+)\}_{10^+} + \epsilon_1\{\nu(8^+) \times \pi(2^+)\}_{10^+} \tag{1}$$

and the final state:

$$|8^+\rangle = \{\nu(8^+) \times \pi(0^+)\}_{8^+} + \epsilon_2\{\nu(10^+) \times \pi(2^+)\}_{8^+} \tag{2}$$

with the coefficients $\epsilon_1, \epsilon_2 \ll 1$. Sistemich *et al* [55] have already suggested this possible mechanism but they were unable to compare it with the experimental data because the $B(E2)$ value of the $10^+ \rightarrow 8^+$ transition was not known with sufficient precision in ^{132}Te and was totally unknown in the lighter Te isotopes. However, the new data now allow this comparison to be made.

It is easy to show that the $\langle 8^+ \| E2(Te) \| 10^+ \rangle$ matrix element between the Te wavefunctions defined in equations (1) and (2) contains four terms which can be evaluated as a function of the elementary $\langle \nu(8^+) \| E2 \| \nu(10^+) \rangle$ and $\langle \pi(0^+) \| E2 \| \pi(2^+) \rangle$ matrix elements using the recoupling

coefficients defined in [56]. Finally, it is easy to show that the reduced E2 transition probability can be written as

$$B(E2(Te), 10^+ \rightarrow 8+) \sim [\sqrt{B(E2, \nu(10^+ \rightarrow 8^+))} + \epsilon 1.9\sqrt{B(E2, \pi(2^+ \rightarrow 0^+))}]^2 \quad (3)$$

with the additional simplification that $\epsilon_1 = \epsilon_2 = \epsilon$. One observes in equation (3) that the $B(E2)$ value in Te is now the sum of a neutron and a proton contribution. These values can be approximated by the experimental $B(E2(Sn), 10^+ \rightarrow 8^+)$ value taken from the Sn isotopes having the same neutron numbers as the Te isotopes and the $B(E2(\mathrm{Te}), 2^+ \rightarrow 0^+)$ value taken from the same Te nucleus. The latter $B(E2)$ value is much larger than the former (which occurs in a magic nucleus). Therefore, even a rather small mixing amplitude can lead to a large enhancement of the total $B(E2)$ value for the $10^+ \rightarrow 8^+$ transitions in Te. In fact, it has been found that the values $\epsilon = 0.08$–0.17 are sufficient to reproduce a very strong enhancement of the $B(E2)$ values as observed experimentally from Sn to Te. In contrast, the calculated energy shifts of the 8^+ and 10^+ states in Te isotopes due to the p–n residual interaction are always smaller than 20 keV, which indicates that the energies of these levels are only affected very weakly by the mixing.

An effect of the same nature was also observed by Genevey *et al* [54] for the nuclei with 50 and 52 neutrons. In figure 21(B), $(B(E2); 8^+ \rightarrow 6^+)$ values of the $\pi g^n_{9/2}$, $\nu = 2$ dominant configuration of the $N = 50$ [57] and $N = 52$ isotones [58–60] are plotted against charge number Z. For $N = 50$ odd-A nuclei [61, 62] of $\pi g^n_{9/2}$, $\nu = 3$ dominant configuration, the $(B(E2); 21/2^+ \rightarrow 17/2^+)$ values are corrected according to the different geometric factors entering the $\nu = 2$ and $\nu = 3$ seniority values and are also plotted in the same figure. The curve obtained is comparable to the one already plotted for the Sn isotopes. Here also, the two values corresponding to the $N = 52$ isotones present a large enhancement of their $B(E2)$ strengths compared to the semi-magic $N = 50$ isotones. This effect is qualitatively analogous to the observed $B(E2)$ enhancement from Sn to Te isotopes.

In conclusion, the proposed mechanism is able to explain the large observed difference in the behaviour of the $B(E2)$ between semi-magic nuclei and nuclei having two neutrons or protons outside a closed shell. This mechanism shows how the collectivity present in low-spin levels spreads to high-spin states. It also shows that only the $B(E2)$ strengths are strongly affected. One may conjecture that this feature is more general and is most likely present in other closed-shell regions of the nuclear chart, where, at present, no experimental information is available.

6. Conclusions

It has been shown in this review that recoil-fragment spectrometers have played a leading role in the search for microsecond isomers in very neutron-rich nuclei close to ^{78}Ni and ^{132}Sn. This technique is very powerful because it allows detection and identification in-flight of isomers which are produced at a very low rate. This feature is of fundamental importance very far from the stability line, where the production yields are very small. It was pioneered at Jülich with the spectrometer JOSEF, in the early seventies. This field was revived in the mid-nineties with the new facilities FRS at GSI, LISE3 at GANIL and the upgraded version of LOHENGRIN at ILL. All these different facilities used different reactions and beam energies to produce the isomers, which makes them complementary. For the moderately neutron-rich nuclei of these mass regions, deep-inelastic binary reactions combined with large γ-detector arrays is the most powerful technique to search for and to study the decay of microsecond isomers.

These new data have considerably increased the nuclear structure information of the nuclei of these two mass regions. They provide the opportunity of testing the predictive power of the shell model far away from the stability line. In the vicinity of ^{132}Sn the agreement between the experimental data and the theory obtained by the Napoli group using realistic effective interactions is very impressive. Moreover, the excitation energies of the last known even–even nucleus ^{134}Sn, characterized by a very low energy 2^+ level of 725 keV, are also well reproduced by the theory.

In contrast, the structure of the nuclei close to ^{78}Ni is not fully understood. The discovery of an 8^+ microsecond isomer in ^{78}Zn strongly suggests that the $N = 50$ neutron gap persists at ^{78}Ni. However, the drop in energy of the 2^+ level from ^{70}Ni to ^{72}Ni is not easy to explain in the framework of the shell model. Moreover, the situation is complicated by the absence of the 8^+ isomers in ^{70}Ni and ^{72}Ni. A possible explanation of this unusual feature was proposed by Grawe *et al*, but it strongly depends on the ingredients of the shell model used in the calculations. In conclusion, more experimental data are necessary in this region. Most likely, knowledge of the origin of the recently measured isomer in ^{76}Ni will strongly help to clarify the nuclear structure of the nuclei in this mass region.

A considerable number of reduced transition probabilities have been measured in the works described in this review. This information was used as a complementary test of the shell model in the vicinity of the doubly magic shells. Moreover, the experimental $B(E2)$ values of $10^+ \rightarrow 8^+$ transitions were compared in the even–even Sn and Te nuclei. Although the experimental data are still incomplete, especially in Te isotopes, it is already possible to observe a strong increase of the $E2$ strength in the Te isotopes compared to the semi-magic Sn isotopes. The mechanism responsible for this effect was identified and is most likely present in other regions of the nuclear chart. It shows how the collectivity present in low-spin states spreads to high-spin states.

Acknowledgments

A part of the experimental results presented in this review was measured at ILL with the LOHENGRIN recoil-fragment spectrometer. It is a pleasure to thank all the colleagues of the ILL team, H R Faust, R Orlandi, A Scherillo, G S Simpson and I Tsekhanovich. The authors are thankful to M Asghar, A Covello, R Grzywacz, M G Porquet and W Urban for comments and discussions.

References

[1] Fogelberg B, Heyde K and Sau J 1981 *Nucl. Phys.* A **352** 157
[2] De Geer L-E and Holm G B 1980 *Phys. Rev.* C **22** 2163
[3] Apt K E and Walters W B 1971 *Phys. Rev. Lett.* **26** 1189
[4] Kanbe M and Kitao K 2001 *Nucl. Data Sheets* **94** 227
[5] Fogelberg B *et al* 1998 *Proc. 2nd Workshop on Nuclear Fission and Fission Products Spectroscopy (Seyssins, France) (AIP Conf. Proc. 447)* ed G Fioni, H Faust, S Oberstedt and F-J Hambsh (Woodbury, NY: AIP) p 191
[6] Zhang C T *et al* 1997 *Z. Phys.* A **358** 9
[7] Gautherin C *et al* 1998 *Eur. Phys. J.* A **1** 391
[8] Houry M 2000 *Thesis* Université de Paris XI Orsay *(Saclay Report DAPNIA/SPHN-00-01-T)*
[9] Broda R *et al* 1992 *Phys. Rev. Lett.* **68** 1671
[10] Mayer R H *et al* 1994 *Phys. Lett.* B **336** 308
[11] Daly P J *et al* 1995 *Phys. Scr.* T **56** 94
[12] Zhang C T *et al* 2000 *Phys. Rev.* C **62** 057305
[13] Zhang C T *et al* 1998 *Nucl. Phys.* A **628** 386

[14] Grüter J W *et al* 1970 *Phys. Lett.* B **33** 474
[15] Grzywacz R *et al* 1995 *Phys. Lett.* B **355** 439
[16] Lewitowicz M *et al* 2001 *Nucl. Phys.* A **682** 175c
[17] Mineva M N *et al* 2001 *Eur. Phys. J* A **11** 9
[18] Pinston J A *et al* 2000 *Phys. Rev.* C **61** 024312
[19] Genevey J *et al* 2000 *Eur. Phys. J* A **9** 191
[20] Genevey J *et al* 2003 *Phys. Rev.* C **67** 054312
[21] Genevey J *et al* 2002 *Phys. Rev.* C **65** 034322
[22] Grzywacz R *et al* 1998 *Phys. Rev. Lett.* **81** 766
[23] Daugas J M *et al* 2000 *Phys. Lett.* B **476** 213
[24] Grzywacz R 2002 *Proc. 3rd Conf. on Fission and Properties of Neutron-Rich Nuclei (Sanibel Island, FL)* to be published
[25] Lewitowicz M 2003 *Nucl. Phys.* A **722** 67c
[26] Huck H *et al* 1989 *Phys. Rev.* C **39** 997
[27] Genevey J *et al* 1998 *Proc. Conf. ENAM 98: Exotic Nuclei and Atomic Masses (Bellaire, MI) (AIP Conf. Proc. 455)* ed B M Sherril, D J Morissey and C N Davids (Woodbury, NY: AIP) p 694
[28] van Poelgeest A *et al* 1980 *Nucl. Phys.* A **346** 70
[29] Lunardi S *et al* 1987 *Z. Phys.* A **328** 487
[30] Lauppe W-D *et al* 1978 *J. Phys. Soc. Japan Suppl.* **44** 335
[31] Björnstad T *et al* 1985 *Nucl. Phys.* A **453** 463
[32] Korgul A *et al* 2000 *Eur. Phys. J.* A **7** 167
[33] Genevey J *et al* 2000 *Eur. Phys. J* A **7** 463
[34] Urban W *et al* 2000 *Phys. Rev.* C **62** 027301
[35] Genevey J *et al* 2001 *Phys. Rev.* C **63** 054315
[36] Walters W B and Stone C A 1994 *Proc. Workshop on Nuclear Fission and Fission Product-Spectroscopy (Seyssins, France) (ILL Report No 94FA05T p.182)* ed H Faust and D Fioni p 182
[37] Kuo T T S and Brown G E 1966 *Nucl. Phys.* **85** 40
[38] Talmi I 1993 *Simple Models of Complex Nuclei: The Shell Model and Interacting Boson Model* (Harwood, NY: Academic) p 401
[39] Grawe H *et al* 2002 *Nucl. Phys.* A **704** 221c
[40] Sinatkas J *et al* 1992 *J. Phys. G: Nucl. Part. Phys.* **18** 1377
[41] Grawe H 1999 *Proc. Workshop on the Beta-Decay, from Weak Interaction to Nuclear Structure (Strasbourg, France)* ed Ph Dessagne, A Michalon and C Miehe p 211
[42] Grzywacz R *et al* 2003 *Proc. Conf. on Frontiers of Nuclear Structure (Berkley, CA) (AIP Conf. Proc. 656)* ed P Fallon and R Clark (Woodbury, NY: AIP) p 233
[43] Insolia A *et al* 1992 *Nucl. Phys.* A **550** 34
[44] Holt A *et al* 1998 *Nucl. Phys.* A **634** 41
[45] Covello A *et al* 1998 *Proc. 6th Spring Seminar on Nuclear Physics: Highlights of Modern Nuclear Structure (S. Agata sui due Golfi, Italy)* ed A Covello (Singapore: World Scientific) p 129
[46] Andreozzi F *et al* 1997 *Phys. Rev.* C **56** R16
[47] Coraggio L *et al* 2002 *Phys. Rev.* C **66** 064311
[48] Coraggio L *et al* 2002 *Phys. Rev.* C **65** 051306
[49] Coraggio L *et al* 1998 *Phys. Rev.* C **58** 3346
[50] Fogelberg B and Blomqvist J 1984 *Phys. Lett.* B **137** 20
[51] Hannawald M *et al* 2000 *Phys. Rev.* C **62** 054301
[52] Mach H *et al* 1995 *Phys. Rev.* C **51** 500
[53] Bhattcharyya P *et al* 2001 *Phys. Rev.* C **64** 054312
[54] Genevey J *et al* 2001 *Proc. 5th Int. Conf. on Dynamical Aspects of Nuclear Fission (Castá-Papiernicka, Slovak Republic)* ed J Kliman, M G Itkis and S Gmuca (New Jersey: World Scientific) p 362
[55] Sistemich K *et al* 1979 *Z. Phys.* A **292** 145
[56] de-Shalit Talmi 1963 *Nuclear Shell Theory* (New York: Academic) p 522
[57] Górska M *et al* 1997 *Phys. Rev. Lett.* **79** 2415
[58] Lederer C M *et al* 1971 *Nucl. Phys.* A **169** 449
[59] Clark R M *et al* 2000 *Phys. Rev.* C **61** 044311
[60] Górska M *et al* 1994 *Z. Phys.* A **350** 181
[61] Alber D *et al* 1990 *Z. Phys.* A **335** 265
[62] Baglin C D *et al* 1997 *Nucl. Data Sheets* **80** 1